Simple Approaches to Correct for Partial-Volume Effect

In the following, the term lesion refers to both the spherical inserts of the tumor phantoms or the tumor within the patient. Of note, in clinical tumor dosimetry, the mean imaged activity concentration within the tumor boundary is commonly used to derive the (mean) tumor absorbed (radiation) dose. When using the mean activity concentration, a partial volume effect correction is necessary in any case unless the objects are extremely large, that is, an equivalent sphere diameter of ≥47 times PET spatial resolution (*1*). There are two simple approaches applied in this study to correct for this effect: a contour- and an oversize-based approach.

Contour-based approach. The contour-based approach uses sphere recovery coefficient (RC) values to correct the mean imaged activity concentration within the lesion boundary, that is, the mean imaged activity concentration (C_{imaged}) was divided by the diameter-dependent RC value and termed contour-based corrected activity concentration. The sphere RC values were derived from the NEMA tumor phantom images.

$$C_{\text{corrected}} = \frac{C_{\text{imaged}}}{RC(d)}$$

It is $C_{\text{corrected}}$ the contour-corrected activity concentration. In the application, the tumor geometry is assumed to be a volume-equivalent sphere with an effective diameter d.

Oversize-based approach. For the oversize-based approach, the total activity (A_{oversize}) within the lesion volume (V_{lesion}) is determined using an oversized VOI (V_{oversize}), that is, the points of the oversize VOI have an approximate distance of one time the PET spatial resolution of the actual geometrical boundary of the lesion. It is assumed that this oversize VOI (with its volume V_{oversize}) contained the main activity to compensate for partial-volume effects; however, the oversize VOI contains contribution from a background activity and requires a correction. The background subtraction can be conducted as follows (*2*):

$$C_{\text{corrected}} = \frac{A_{\text{oversize}} - \left(V_{\text{oversize}} - V_{\text{lesion}}\right) \cdot C_{\text{bgr}}}{V_{\text{lesion}}}$$

It is $C_{\text{corrected}}$ and C_{bgr} the oversize-corrected and background activity concentration, respectively. The background activity concentration is the local background derived from a representative background VOI close to the lesion. Of note, this approach assumes a uniform background activity concentration.

Activity Measurements

Three independent vial geometries – 10-mL TEMA syringe, 10-mL Becton & Dickinson syringe (B&D), 11-mL TechneVial – were used to measure the ^{90}Y activity in two different dose calibrators (CRC-25R and CRC-15R, Capintec Inc., Ramsey, NJ, USA). Each vial geometry was calibrated by a metrology institution. The mean of these activity concentration measurements along with their 95% confidence level was calculated and used to determine the reference activity concentration and its maximum error. The reference activity concentration and error estimate was 3.58 MBq/mL ±7% at the 95%-confidence level (Supplemental Table S1).

PET/CT System

The digital PET/CT system used for phantom and patient examinations was a Biograph Vision 600 PET/CT scanner (Siemens Healthineers, Erlangen, Germany). Detailed scanner specifications were published elsewhere (*3*) and are summarized in Supplemental Table S2. For this system, the branching ratio related to the internal pair production of ^{90}Y and the ^{90}Y half-life were 0.0032% and 64.053 h, respectively.

Phantoms

Setup and preparation

Tumor phantoms. Two types of tumor phantoms were used. First, the NEMA tumor phantom (NEMA IEC/2001 body phantom) is a torso-shaped phantom (torso volume of 9720 mL) containing 6 spheres (diameters: 9.7, 12.6, 17.4, 22.2, 27.7, and 37.0 mm) to simulate hot lesions in a uniform warm background. Second, the anthropomorphic abdominal tumor phantom (Abdo-Man) was originally designed for quantitative imaging analysis of selective internal radiation therapy (*4*). The phantom contains a refillable liver insert (inner volume of 1768 mL), in which 4 spheres (diameters: 10.0, 20.0, 30.0, and 40.0 mm) are attached. It was selected from the phantoms available in our institution to resemble the human body scattering geometry more realistically than the NEMA tumor phantom.

Preparation. Based on clinical data, the spherical inserts and the cavity were filled with ^{90}Y in aqueous solution at a representative initial sphere activity concentration of about 3.3 MBq/mL and a signal-to-background ratio of about 40 at PET start time. To prevent binding of ^{90}Y to the phantom and sphere walls, the chelator DTPA was added in excess to the ^{90}Y solution; acetate buffer was used to adjust a pH value of about 6.5. PET imaging was performed directly following preparation and at 7 additional time points spaced approximately one ^{90}Y half-life apart to investigate the quantification accuracy at varying activity concentration values. The activity concentrations at PET start time were 3.36, 1.96, 1.22, 0.73, 0.34, 0.20, 0.12, and 0.05 MBq/mL for the NEMA tumor phantom and 3.33, 1.97, 1.23, 0.73, 0.34, 0.20, 0.12, and 0.06 MBq/mL for the anthropomorphic tumor phantom.

PET acquisition

All phantom PET data were acquired using a single-bed position on a digital Biograph Vision 600 PET/CT scanner (Siemens Healthineers, Erlangen, Germany). Initially, the NEMA tumor phantom

was scanned for 6 h and the resulting images were used to determine the recovery coefficients at high counting statistics. Thereafter, PET data of both phantoms were acquired for 30 min and used to reconstruct PET images using the total 30-min and 15-min acquisition time data. For attenuation correction, a low-dose CT scan was acquired (Care DOSE 4D, quality reference 160 mAs; CARE kV, quality reference 120 kV).

Image reconstruction

Images were reconstructed using three-dimensional ordinary Poisson ordered-subset expectation maximization (OSEM) with time-of-flight option (TOF) and with point-spread-function (PSF) modelling as previously recommended for quantitative ^{90}Y PET imaging on the Biograph Vision using 3 iterations and 5 subsets (*5*). Two post-reconstruction smoothing filter levels (all-pass and 5-mm Gaussian filter) were applied. The images had an almost cuboid-shaped voxel size with side lengths of 3.30x3.30x3.00 mm^3.

System spatial resolution measurements

The detailed description of the resolution phantom has been published by our group (*6*). Briefly, a cylindrical phantom (20 cm axial length, 20 cm outside diameter) contained line sources orthogonal to the transverse plane (or parallel to the PET system axis). The cavity of the phantom was filled with non-radioactive water. The line source, consisting of a refillable polyethylene tubing (0.5-mm inner diameter), was looped back through the phantom to provide four distances of 1 and 7 cm from the central axis of the scanner's field of view (FOV): (x = 1 cm, y = 0), (x = 7 cm, y = 0), (x = 0, y = 1 cm), (x = 0, y = 7 cm). The transverse spatial resolution was determined at four positions each at the center (z = 0) and one-fourth of the scanner's FOV (z = ±1/4 FOV). The selected total activity in the line sources was 400–600 MBq.

The acquisition duration was 2 h and the resulting images were reconstructed using three-dimensional ordinary Poisson ordered-subset expectation maximization (OSEM) with TOF option and with PSF modelling as previously recommended for quantitative ^{90}Y PET imaging on the

Biograph Vision using 3 iterations and 5 subsets (*5*). The images had an almost cuboid-shaped voxel size with side lengths of 0.83 x 0.83 x 3.00 mm^3. Two smoothing filter levels (all-pass and 5-mm Gaussian filter) were applied. The measured system spatial resolution (average full width at half maximum) was 3.3 mm for all-pass and 6.0 mm for a 5-mm Gaussian smoothing filter.

Patients

Patient characteristics

Retrospective analysis of clinical data was approved by the local Ethics Committee (permits no. 20-9558-BO). Data sets of three patients were included, who suffered from progressive, advanced-stage solitary fibrous tumor (SFT) and received a first cycle of ^{90}Y-FAPI-46 therapy under compassionate access following clinical indication. Radionuclide treatment was decided for in a multidisciplinary tumor board. All patients had either previously shown progressive disease during established treatment options or were not eligible for other established treatment concepts. The administered therapeutic activities were 8.90 GBq (patient#1), 3.82 GBq (patient#2), and 3.6 GBq (patient#3). Patient masses were 82 kg (patient#1), 51 kg (patient#2), and 51 kg (patient#3). Activities were determined using the 10-mL TEMA syringe geometry.

PET acquisition

PET/CT examinations were scheduled in reference to a previous study (*7*). PET data were acquired using two bed positions with 15 min acquisition time per bed position. Because of symptomatic patients and logistical reasons, serial PET/CT acquisition was performed at slightly differing time points: 17, 22, 41 hours p.i. for patient #1, 2, 20, 43 hours p.i. for patient #2, and 1, 4, 20 hours p.i. for patient #3.

Image reconstruction

Images were reconstructed using the image reconstruction algorithm and the respective parameters (Poisson-OSEM PSF-TOF, iterations, voxel size) as described in the phantom section except for the smoothing level. For patient images, a 5-mm Gaussian smoothing filter was applied based on the phantom results. For attenuation correction, low-dose CTs were acquired (see above).

Phantom analysis

Mean recovery coefficients

NEMA tumor phantom PET data acquired for 6 hours were used to determine the mean RC values. The measured RC value (RC_{msd}) for each sphere was calculated by the ratio of the mean imaged activity concentration within the sphere boundary to the true activity concentration (using the dose calibrator-based value). A 3-parameter sigmoidal function was applied to fit the measured RC values as a function of the sphere diameter (d):

$$RC_{\text{fit}} = a \cdot \left[1 + e^{-b \cdot (d - d_o)}\right]^{-1}$$

The symbols a, b, and d_0 are fitting parameters.

The estimated fitting parameters were a = 0.87, b = 0.35 mm^{-1}, d_0 = 9.34 mm for the non-filtered images and a = 0.81, b = 0.27 mm^{-1}, d_0 = 10.86 mm for the 5-mm Gaussian filtered images. Measured and fitted RC values for the different sphere size diameters of both tumor phantoms are listed in Supplemental Table S3.

Minimum detectable activity concentration

The images of the NEMA tumor phantom at varying activity concentration values were used to determine the minimum detectable activity concentration. Its determination has been previously described (*8*). In brief, first, the visual detectability of each sphere was determined in a human

observer study (triple read). The detectability level was assessed using a three-point scale from "0" to "2". Spheres with a sum score of ≥3 were regarded as "detected" unless a single rating for a lesion was "0" (*9*). Second, the signal-to-noise ratio (*SNR*) of each sphere was determined:

$$SNR = \frac{C_{\text{imaged}} - C_{\text{bgr}}}{\sigma_{\text{bgr}}}$$

The symbols C_{imaged}, C_{bgr}, and σ_{bgr} represent the mean sphere activity concentration, the background activity concentration, and the standard deviation of the phantom background, respectively. The background activity concentration was determined using 19 spherical VOIs with a diameter of 37.0 mm (corresponding to the diameter of the largest sphere of the phantom insert) placed at random positions. Third, visual detectability level and SNR were correlated in a histogram analysis to estimate the SNR threshold indicating detectability. Finally, the SNR was evaluated as a function of the activity concentration. Thereafter, the minimum detectable activity concentration was calculated for each sphere using the respective activity concentration at the threshold SNR.

Quantification accuracy evaluation

For a more realistic simulation of the scattering geometry of the human abdomen, the anthropomorphic abdominal tumor phantom was investigated. The anthropomorphic abdominal tumor phantom was applied to evaluate the activity concentration quantification accuracy as a function of activity concentration levels using the contour- and oversize-based approaches. To evaluate the lesion quantification accuracy, the activity concentration ratios of PET-imaged to (decay corrected) dose calibrator-derived measurements were determined.

In the evaluation, a ±20% deviation range of the activity concentration ratio was regarded acceptable. This deviation range considered the overall maximum estimated uncertainty at 95%-confidence interval for (a) the ^{90}Y activity concentration measurement of ±7%, (b) a ^{18}F PET cross-

calibration measurement of ±6% (*10*) and (c) the frequency of the positron-electron pair conversion of ±5% (*11-14*).

Minimum quantifiable activity concentration

The results of the quantification accuracy evaluations were used to estimate the minimum quantifiable activity concentration of reliability, that is, above that minimum quantifiable activity concentration the quantification appears to be reliable. In the derivation, the values of the quantification accuracy should lie within the ±20% deviation range.

Patient Analysis

In the patient analysis, key quantities related to the estimation of the tumor absorbed dose were derived. The procedure has previously been described (*7*). Briefly, the tumor volumes were estimated by manual segmentation (VOI technique) using the respective CT images and the VOIs were used to determine the tumor uptake values at three imaging time points. Mean tumor activity concentrations were determined using both the contour-based and the oversize-based approach. The resulting uptake curves were parameterized by fitting a mono-exponential function to the measured uptake values to determine the effective half-lives. The time-integrated activity coefficients (residence times) were determined and used to estimate the tumor absorbed doses using the sphere model of OLINDA/EXM (*15*).

Comparison of minimum detectable activity concentration between NEMA and anthropomorphic phantoms

For the anthropomorphic phantom, the human observer study revealed a SNR threshold of ≥7 to distinguish between “not-detected” and “detected” spheres. The minimum detectable activity concentration for each sphere size is shown in Supplemental Table S4. The 5-mm smoothed images provided an improved detectability for smaller spheres and the minimum detectable

activity concentration was smaller by a mean factor of 0.54 compared to images without Gaussian smoothing. For a 30-min acquisition time, the minimum detectable activity concentration was reduced by a factor of 0.46 compared to the 15-min acquisition time.

In comparison to the NEMA phantom, the minimum detectable activity concentration values were mostly slightly higher, probably because of the differing scatter geometry and sphere positioning. The increase in minimum detectable activity concentration was more prominent for the smallest 10-mm sphere at the lower acquisition time of 15 min. We suggest that this is associated with the low absolute amount of ^{90}Y activity in this sphere resulting in poor counting statistics and with the proximity to the 40-mm sphere. Of note, this was also reflected in the investigation of the minimum quantifiable activity concentration of the anthropomorphic phantom (Table 2 in main text). In general, for the anthropomorphic phantom, the minimum detectable activity concentration values were in good agreement with the minimum quantifiable activity concentration values.

Supplemental Tables

Supplemental Table S1 – Activity concentration measurements of three independent geometries

Supplemental Table S1. Overview of the activity concentration measurements of three independent geometries and their respective dose calibrators to estimate the reference activity concentration of 3.58 MBq/mL along with its maximum error estimate of ±7% at the 95% confidence level – B&D activity measurements were considered as one independent measurement.

Geometry[a]	Dose calibrator (setting number)	Filling vol. (mL)	Activity (MBq)	Activity conc. (MBq/mL)	95%-Confidence Interval	Reference[b]
B&D	CRC-15R (52x10)	5.77	19.25	3.36[c]	10%	Siegel *et al.*
B&D	CRC-15R (56x10)	5.77	18.67	3.26[c]	10%	Zimmermann *et al.*
TEMA	CRC-25R (35x10)	7.82	30.04	3.84	3%	Eckert und Ziegler
TechneVial	CRC-15R (48x10)	9.69	34.81	3.59	7%	Vargas *et al.*

[a] 10-mL B&D syringe (Becton & Dickinson, Franklin Lakes, USA) with reference volume of 6 mL; 10-mL TEMA syringe with reference volume of 8 mL (Menny Medical, Mirandola, Italy); 11-mL TechneVial (Mallinckrodt, Staines-Upon-Thames, UK) with reference volume of 10 mL. [b] Siegel *et al.* J Nucl Med 2004,45:450; Zimmermann *et al.* Applied Radiation and Isotops 2004,60:511; calibration measurement performed by Eckert und Ziegler (Berlin, Deutschland); Vargas *et al.* EJNMMI Phys 2020,7:69. [c]As the two activity measurements with the two B&D geometries were considered as one independent measurement, average value of the B&D measurements (3.31 MBq/mL) was calculated first and further used in the determination of the mean activity concentration.

Supplemental Table S2 – Technical specifications for the Biograph Vision 600

Supplemental Table S2. Technical specifications for the Biograph Vision 600.

Detector material	LSO[a]
Detector element dimension ($mm^{3)}$	3.2x3.2x20
Detector elements per block	16x16
Total number of detector elements	60,800
Signal readout	SiPM[b] (2x2 per block)
Axial FOV (cm)	26.3
Transaxial FOV (cm)	78
Plane spacing (mm)	1.65
Image planes	119
Coincidence time window (ns)	4.7
Energy window (keV)	435–585
Energy resolution (%)	9
System time resolution (ps)	210
NEMA sensitivity (kcps/MBq)	16.4

[a] LSO, Lutetium oxyorthosilicate. [b] SiPM, silicon-photomultiplier.

Supplemental Table S3 – Measured and fitted recovery coefficients

Supplemental Table S2. Measured (RC_{msd}) and fitted (mean) recovery coefficient (RC_{fit}) of the sphere tumor phantoms for all-pass and 5-mm Gaussian smoothing.

Phantom	Diameter (mm)	All-pass		5-mm smoothing	
		RC_{msd}	RC_{fit}	RC_{msd}	RC_{fit}
NEMA phantom					
	9.7	0.49	0.46	0.35	0.34
	12.6	0.66	0.66	0.52	0.50
	17.4	0.84	0.82	0.69	0.69
	22.2	0.85	0.86	0.76	0.77
	27.7	0.86	0.87	0.79	0.80
	37.0	0.88	0.87	0.83	0.81
	10.0	–	0.49	–	0.36
Anthropomorphic phantom					
	20.0	–	0.85	–	0.75
	30.0	–	0.87	–	0.81
	40.0	–	0.87	–	0.81

Supplemental Table S4 - Minimum detectable activity concentration for the anthropomorphic phantom

Supplemental Table S4. Estimated minimum detectable activity concentration (in MBq/mL) for the anthropomorphic phantom presenting results for the investigated sphere diameters, acquisition time durations (15 min vs. 30 min), and smoothing levels (all-pass vs. 5-mm Gaussian filter).

Diameter	All-pass		5-mm smoothing	
(mm)	15 min	30 min	15 min	30 min
10	1.84	0.31	1.43	0.21
20	0.67	0.40	0.31	0.22
30	0.55	0.27	0.24	0.13
40	0.45	0.23	0.21	0.11

Supplemental Figures

Supplemental Figure S1

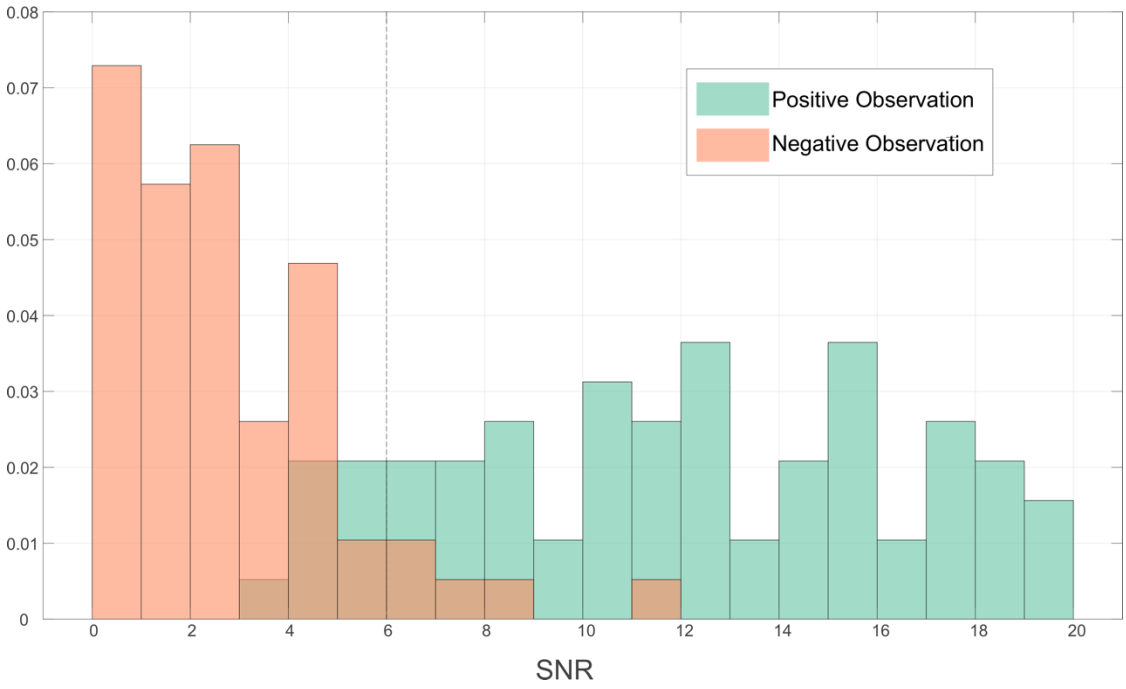

Supplemental Figure S1. Histogram analysis of the human observer study and sphere SNR derived from the NEMA tumor phantom. A threshold of SNR≥6 was determined to indicate detectability (dashed vertical line). For reasons of clarity, detected lesions with SNR larger or equal to 20 are not presented.

Supplemental Figure S2

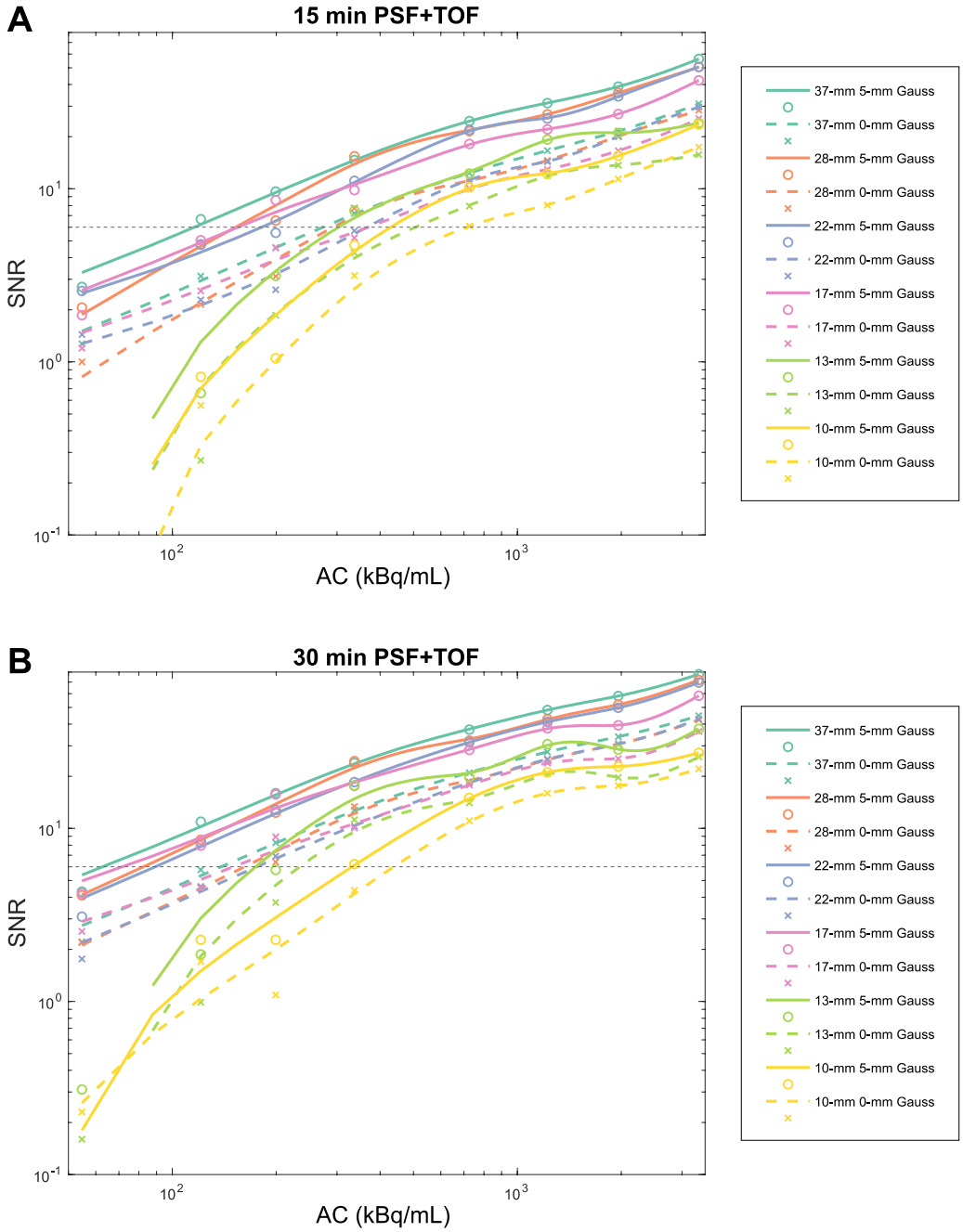

Supplemental Figure S2. SNR as a function of the activity concentration for an acquisition time of 15 min (A) and 30 min (B) derived from the NEMA tumor phantom. Dashed horizontal lines at SNR equals 6 indicate the threshold SNR to estimate the minimum detectable activity concentration.

REFERENCES

<jrn>1. Jentzen W. Experimental investigation of factors affecting the absolute recovery coefficients in iodine-124 PET lesion imaging. *Phys Med Biol*. 2010;55:2365–2398. PubMed</jrn>

<jrn>2. Walrand S, Jamar F, Mathieu I, et al. Quantitation in PET using isotopes emitting prompt single gammas: application to yttrium-86. *Eur J Nucl Med Mol Imaging*. 2003;30:354–361. PubMed</jrn>

<jrn>3. van Sluis J, de Jong J, Schaar J, et al. Performance characteristics of the digital Biograph Vision PET/CT system. *J Nucl Med*. 2019;60:1031–1036. PubMed</jrn>

<jrn>4. Gear JI, Cummings C, Craig AJ, et al. Abdo-Man: a 3D-printed anthropomorphic phantom for validating quantitative SIRT. *EJNMMI Phys*. 2016;3:17. PubMed</jrn>

<jrn>5. Kunnen B, Beijst C, Lam M, Viergever MA, de Jong H. Comparison of the Biograph Vision and Biograph mCT for quantitative ^{90}Y PET/CT imaging for radioembolisation. *EJNMMI Phys*. 2020;7:14. PubMed</jrn>

<jrn>6. Jentzen W, Weise R, Kupferschlager J, et al. Iodine-124 PET dosimetry in differentiated thyroid cancer: recovery coefficient in 2D and 3D modes for PET(/CT) systems. *Eur J Nucl Med Mol Imaging*. 2008;35:611–623. PubMed</jrn>

<jrn>7. Ferdinandus J, Costa PF, Kessler L, et al. Initial clinical experience with ^{90}Y-FAPI-46 radioligand therapy for advanced-stage solid tumors: a case series of 9 patients. *J Nucl Med*. 2022;63:727–734. PubMed</jrn>

<jrn>8. Kersting D, Jentzen W, Fragoso Costa P, et al. Silicon-photomultiplier-based PET/CT reduces the minimum detectable activity of iodine-124. *Sci Rep*. 2021;11:17477. PubMed</jrn>

<jrn>9. Øen SK, Aasheim LB, Eikenes L, Karlberg AM. Image quality and detectability in Siemens Biograph PET/MRI and PET/CT systems: a phantom study. *EJNMMI Phys*. 2019;6:16. PubMed</jrn>

<jrn>10. Keller SH, Jakoby B, Svalling S, Kjaer A, Hojgaard L, Klausen TL. Cross-calibration of the Siemens mMR: easily acquired accurate PET phantom measurements, long-term stability and reproducibility. *EJNMMI Phys*. 2016;3:11. PubMed</jrn>

<jrn>11. Dryák P, Solc J. Measurement of the branching ratio related to the internal pair production of Y-90. *Appl Radiat Isot*. 2020;156:108942. PubMed</jrn>

<eref>12. Chistsé V, Bé MM. ^{90}Y: comments on evaluation of decay data. Decay Data Evaluation Project website. http://www.nucleide.org/DDEP_WG/Nuclides/Y-90_com.pdf. Updated November 2016. Accessed March 3, 2022.</eref>

<jrn>13. Staníček J. Emission of positrons in beta-decay of ^{90}Sr + ^{90}Y. *Acta Phys Univ Comen*. 2007;•••:51–56.</jrn>

<jrn>14. Selwyn RG, Nickles RJ, Thomadsen BR, DeWerd LA, Micka JA. A new internal pair production branching ratio of ^{90}Y: the development of a non-destructive assay for ^{90}Y and ^{90}Sr. *Appl Radiat Isot*. 2007;65:318–327. PubMed</jrn>

<jrn>15. Stabin MG, Sparks RB, Crowe E. OLINDA/EXM: the second-generation personal computer software for internal dose assessment in nuclear medicine. *J Nucl Med*. 2005;46:1023–1027. PubMed</jrn>